Eur. Phys. J. C 54, 411–423 (2008)
DOI 10.1140/epjc/s10052-008-0547-0

THE EUROPEAN PHYSICAL JOURNAL C

Regular Article – Experimental Physics

New high statistics measurement of K_{e4} decay form factors and $\pi\pi$ scattering phase shifts[a]

The NA48/2 Collaboration

J.R. Batley[1], A.J. Culling[1], G. Kalmus[1], C. Lazzeroni[1,19], D.J. Munday[1], M.W. Slater[1], S.A. Wotton[1], R. Arcidiacono[2,14], G. Bocquet[2], N. Cabibbo[2,20], A. Ceccucci[2], D. Cundy[2,21], V. Falaleev[2], M. Fidecaro[2], L. Gatignon[2], A. Gonidec[2], W. Kubischta[2], A. Norton[2,6], A. Maier[2], M. Patel[2], A. Peters[2], S. Balev[3], P.L. Frabetti[3], E. Goudzovski[3,22], P. Hristov[3,2], V. Kekelidze[3], V. Kozhuharov[3], L. Litov[3], D. Madigozhin[3], E. Marinova[3], N. Molokanova[3], I. Polenkevich[3], Y. Potrebenikov[3], S. Stoynev[3], A. Zinchenko[3], E. Monnier[4,16], E. Swallow[4], R. Winston[4], P. Rubin[5,23], A. Walker[5], W. Baldini[6], A. Cotta Ramusino[6], P. Dalpiaz[6], C. Damiani[6], M. Fiorini[6], A. Gianoli[6], M. Martini[6], F. Petrucci[6], M. Savrié[6], M. Scarpa[6], H. Wahl[6], A. Bizzeti[7,17], M. Calvetti[7], E. Celeghini[7], E. Iacopini[7], M. Lenti[7], F. Martelli[7,18], G. Ruggiero[7,22], M. Veltri[7,18], M. Behler[8], K. Eppard[8], K. Kleinknecht[8], P. Marouelli[8], L. Masetti[8,24], U. Moosbrugger[8], C. Morales Morales[8], B. Renk[8], M. Wache[8], R. Wanke[8], A. Winhart[8], D. Coward[9,25], A. Dabrowski[9], T. Fonseca Martin[9,2], M. Shieh[9], M. Szleper[9], M. Velasco[9], M.D. Wood[9,26], G. Anzivino[10], P. Cenci[10], E. Imbergamo[10], A. Nappi[10], M. Pepe[10], M.C. Petrucci[10], M. Piccini[10], M. Raggi[10], M. Valdata-Nappi[10], C. Cerri[11], G. Collazuol[11], F. Costantini[11], L. DiLella[11], N. Doble[11], R. Fantechi[11], L. Fiorini[11], S. Giudici[11], G. Lamanna[11], I. Mannelli[11], A. Michetti[11], G. Pierazzini[11], M. Sozzi[11], B. Bloch-Devaux[12,b], C. Cheshkov[12,2], J.B. Chèze[12], M. De Beer[12], J. Derré[12], G. Marel[12], E. Mazzucato[12], B. Peyaud[12], B. Vallage[12], M. Holder[13], M. Ziolkowski[13], S. Bifani[14], C. Biino[14], N. Cartiglia[14], M. Clemencic[14,2], S. Goy Lopez[14,2], F. Marchetto[14], H. Dibon[15], M. Jeitler[15], M. Markytan[15], I. Mikulec[15], G. Neuhofer[15], L. Widhalm[15]

[1] Cavendish Laboratory, University of Cambridge, Cambridge, CB3 0HE, UK[c]
[2] CERN, 1211 Genève 23, Switzerland
[3] Joint Institute for Nuclear Research, 141980 Dubna, Russian Federation
[4] The Enrico Fermi Institute, The University of Chicago, Chicago, IL 60126, USA
[5] Department of Physics and Astronomy, University of Edinburgh, JCMB King's Buildings, Mayfield Road, Edinburgh, EH9 3JZ, UK
[6] Dipartimento di Fisica dell'Università e Sezione dell'INFN di Ferrara, 44100 Ferrara, Italy
[7] Dipartimento di Fisica dell'Università e Sezione dell'INFN di Firenze, 50125 Firenze, Italy
[8] Institut für Physik, Universität Mainz, 55099 Mainz, Germany[d]
[9] Department of Physics and Astronomy, Northwestern University, Evanston, IL 60208-3112, USA
[10] Dipartimento di Fisica dell'Università e Sezione dell'INFN di Perugia, 06100 Perugia, Italy
[11] Dipartimento di Fisica dell'Università, Scuola Normale Superiore e Sezione dell'INFN di Pisa, 56100 Pisa, Italy
[12] DSM/DAPNIA – CEA Saclay, Bât 141, 91191 Gif-sur-Yvette Cedex, France
[13] Fachbereich Physik, Universität Siegen, 57068 Siegen, Germany[e]
[14] Dipartimento di Fisica Sperimentale dell'Università e Sezione dell'INFN di Torino, 10125 Torino, Italy
[15] Österreichische Akademie der Wissenschaften, Institut für Hochenergiephysik, 10560 Wien, Austria[f]
[16] Centre de Physique des Particules de Marseille, IN2P3-CNRS, Université de la Méditerranée, Marseille, France
[17] Istituto di Fisica, Università di Modena, 41100 Modena, Italy
[18] Istituto di Fisica, Università di Urbino, 61029 Urbino, Italy
[19] University of Birmingham, Edgbaston, Birmingham, B15 2TT, UK
[20] Università di Roma "La Sapienza" e Sezzione dell'INFN di Roma, 00185 Roma, Italy
[21] Istituto di Cosmogeofisica del CNR di Torino, 10133 Torino, Italy
[22] Scuola Normale Superiore and INFN, 56100 Pisa, Italy
[23] Department of Physics and Astronomy, George Mason University, Fairfax, VA 22030, USA
[24] Physikalisches Institut, Universität Bonn, 53115 Bonn, Germany
[25] SLAC, Stanford University, Menlo Park, CA 94025, USA
[26] UCLA, Los Angeles, CA 90024, USA

Received: 29 October 2007 / Revised version: 24 January 2008 /
Published online: 19 February 2008 –

Abstract. We report results from a new measurement of the K_{e4} decay $K^{\pm} \to \pi^+\pi^- e^{\pm}\nu$ by the NA48/2 collaboration at the CERN SPS, based on a partial sample of more than 670 000 K_{e4} decays in both charged modes collected in 2003. The form factors of the hadronic current (F, G, H) and $\pi\pi$ phase difference $(\delta = \delta_s - \delta_p)$ have been measured in ten independent bins of the $\pi\pi$ mass spectrum to investigate their variation. A sizeable acceptance at large $\pi\pi$ mass, a low background and a very good resolution contribute to an improved experimental accuracy, a factor two better than in the previous measurement, when extracting the $\pi\pi$ scattering lengths a_0^0 and a_0^2. Under the assumption of isospin symmetry and using numerical solutions of the Roy equations, the following values are obtained in the plane $\left(a_0^0, a_0^2\right)$: $a_0^0 = 0.233 \pm 0.016_{\rm stat} \pm 0.007_{\rm syst}$, $a_0^2 = -0.0471 \pm 0.011_{\rm stat} \pm 0.004_{\rm syst}$. The presence of potentially large isospin effects is also considered and will allow comparison with precise predictions from Chiral Perturbation Theory.

PACS. 13.20.Eb; 13.75.Lb

1 Introduction

The study of $K^{\pm} \to \pi^+\pi^- e^{\pm}\nu$ decays (K_{e4}) is of particular interest as it gives access to the final state interaction of two pions in absence of any other hadron. The asymmetry of the dilepton system with respect to the dipion system is related to the difference δ between the s- and p-wave $\pi\pi$ scattering phases for isospin states 0 and 1 $\left(\delta_0^0 - \delta_1^1\right)$. Under the assumption of isospin symmetry, the measured variation of the phase shift with the invariant mass $M_{\pi\pi}$ near threshold can be related to a_0^0 and a_0^2 (the $\pi\pi$ s-wave scattering lengths for isospin states 0 and 2) using dispersion relations based on general properties like analyticity, unitarity and crossing symmetry (known as "Roy equations" [1]). Numerical solutions of these relations, including experimental input data at intermediate energies, have been developed in the past years [2, 3]. Additional constraints from Chiral Perturbation Theory (ChPT) lead to quite precise predictions for the scattering length values [4] $\left(a_0^0 = 0.220 \pm 0.005, a_0^2 = -0.0444 \pm 0.0010\right)$ and for the behavior of the K_{e4} hadronic form factors near threshold [5].

In the past years, only two experiments collected significant samples of K_{e4} decays [6–8], large enough to study their properties but without reaching yet the same precision level as the theoretical predictions. The NA48/2 experiment exploits the existing detector used for precise measurements of CP violation effects in neutral kaon decays to investigate similar effects in charged kaon decays into 3π [9, 10]. The high intensity charged kaon beams allow to record at the same time large samples of rare decay modes like K_{e4} with branching fraction of order 10^{-5}. Data have been collected in 2003–2004, providing a sample of more than $10^6 K_{e4}$ decays. The analysis of data statistics recorded in 2003 already brings an experimental precision competitive with the theoretical one and thus a new insight into the comparison with theory predictions.

2 Beam and detector

Two simultaneous K^+ and K^- beams are produced by 400 GeV protons from the CERN/SPS, impinging on a 40 cm long beryllium target. Opposite charge particles, with a momentum of (60 ± 3) GeV/c, are selected by two systems of dipole magnets (each forming an "achromat"), focusing quadrupoles, muon sweepers and collimators. Kaons then decay in a 114 m long vacuum tank, 192 cm diameter in the first 66 m and 240 cm in the last 48 m. The NA48 detector and its performances are described in detail elsewhere [11]. The important components for the K_{e4} analysis are recalled here:

- Charged particle momenta from $K^{\pm}$ decays are measured in a magnetic spectrometer consisting of four drift chambers (DCH) and a large aperture dipole magnet located between the second and third chamber. Each chamber consists of four staggered double planes of sense wires along the horizontal, vertical and $\pm 45°$ directions. The momentum resolution of the spectrometer is $\sigma(p)/p = (1.02 \oplus 0.044p)\%$ (p in GeV/c).
- A liquid-krypton calorimeter (LKr) measures the energy of electrons and photons. The transverse segmentation into 13 248 2 cm × 2 cm projective cells and the 27 radiation length thickness result in an energy resolution $\sigma(E)/E = (3.2/\sqrt{E} \oplus 9.0/E \oplus 0.42)\%$ (E in GeV) and a space resolution for isolated showers $\sigma_x = \sigma_y = (0.42/\sqrt{E} \oplus 0.06)$ cm. This allows to separate electrons ($E/p \sim 1$) from pions ($E/p < 1$).
- A hodoscope consisting of two planes of scintillators segmented into horizontal and vertical strips is used to trigger the detector readout on charged track topologies. Its time resolution is ~ 150 ps.
- A two-level trigger logic selects and flags events with at least 3 tracks forming consistent 2-track vertices with the beam line.
- A beam spectrometer (KABES), based on Micromegas amplification in a TPC [12], allows to measure the in-

[a] This measurement is dedicated to the memory of René Turlay (1932–2002)

[b] e-mail: bbloch@hep.saclay.cea.fr

[c] Funded by the UK Particle Physics and Astronomy Research Council

[d] Funded by the German Federal Minister for Education and research under contract 05HK1UM1/1

[e] Funded by the German Federal Minister for Research and Technology (BMBF) under contract 056SI74

[f] Funded by the Austrian Ministry for Traffic and Research under the contract GZ 616.360/2-IV GZ 616.363/2-VIII, and by the Fonds für Wissenschaft und Forschung FWF Nr. P08929-PHY

cident kaon momentum with a relative precision better than 1%.

3 Event selection

The 2003 data were selected for three well reconstructed charged tracks topologies, in time within 6 ns for the chambers signals and within 2 ns for the corresponding hodoscope signals. Two opposite sign pions ($E/p < 0.8$) and one electron or positron ($0.9 < E/p < 1.1$) were required. In the first spectrometer chamber, the distance between any two tracks should be at least 2 cm and the minimum distance from the beam line at least 12 cm. The 3-track reconstructed vertex position had to lie within a 5 cm radius transverse to the beam line and within 2 to 95 m downstream of the final collimator. The track impact at the LKr front face was required to fall within the active fiducial region, away from any dead cell. The track-to-track distance had to be larger than 20 cm to prevent shower overlaps. A minimum requirement of 3 GeV/c (resp. 5 GeV/c) for the electron (resp. pion) momenta was applied while the maximum momentum sum had to be less than 70 GeV/c. The reconstructed 3-track invariant mass (assigning a pion mass to each track) and the transverse momentum $p_{\rm t}$ relative to the beam axis had to be outside an ellipse centered on the kaon mass and zero $p_{\rm t}$, with semi-axes ± 20 MeV/c^2 and ± 35 MeV/c, allowing missing energy and $p_{\rm t}$ for the undetected neutrino. No more than 3 GeV energy deposits in the calorimeter, not associated to tracks but in-time with the considered track combination, were allowed.

A more precise estimate than the 60 GeV/c average beam momentum is obtained by imposing energy-momentum conservation in kaon decay, under the assumption of a missing neutrino ($E_\nu = |\mathbf{p}_\nu|$) and fixing the kaon mass and the beam direction to their nominal value. This translates into the solutions of a quadratic equation in p_K, the kaon momentum. If a solution exists in the range [50,70] GeV/c, the event is kept and the solution closer to 60 GeV/c is assigned to p_K.

4 Background

The background sources are twofold: $K^\pm \to \pi^+\pi^-\pi^\pm$ decays with subsequent $\pi \to e\nu$ decay or a pion mis-identified as an electron; and $K^\pm \to \pi^\pm\pi^0(\pi^0)$ decays with subsequent Dalitz decay of a $\pi^0(\pi^0_{\rm D} \to e^+e^-\gamma)$ with an electron mis-identified as a pion and photon(s) undetected. The elliptic cut in the plane $(M_{3\pi}, p_{\rm t})$ rejects $K^\pm \to \pi^+\pi^-\pi^\pm$ decays which have very small $p_{\rm t}$ values. Requiring the square missing mass to the $(K^\pm - \pi^\pm)$ system to be larger than $0.04\,({\rm GeV}/c^2)^2$ further rejects $K^\pm \to \pi^\pm\pi^0$ decays. The invariant mass of the e^+e^- system (assigning an electron mass to the opposite charge pion) larger than $0.03\,{\rm GeV}/c^2$ insures rejection of conversion photons and of some multi π^0 events. Additional rejection against pions mis-identified as electrons is achieved by using a dedicated linear discriminant variable (LDA) based on shower properties (E/p, radial shower width and energy weighted track-cluster distance). The training of this variable has been performed on pion tracks from well reconstructed $K_{3\pi}$ events having $E/p > 0.9$ and electron tracks from K_{e3} decays. It provides an almost momentum independent high efficiency for electron tracks and additional rejection of pion tracks. The precise rejection level can be adjusted according to the discriminant variable value.

The ratio of background to signal is kept at the $\sim 0.5\%$ relative level. It is estimated from "wrong sign" (WS) events ($\pi^\pm\pi^\pm e^\mp\nu$), which, assuming the validity of the $\Delta S = \Delta Q$ rule, can only be background. This has been cross-checked using Monte Carlo simulated events from the various topologies. The contribution of background to signal events has the same magnitude as that measured from WS events if originating from $K^\pm \to \pi^\pm\pi^0(\pi^0)$ decays but has to be multiplied by a factor 2 if originating from $K_{3\pi}$ decays because of the two equal charge pions. A total of 677 510 K_{e4} candidates (435 654 K^+ and 241 856 K^-) were selected from $\sim 2 \times 10^9$ charged triggers recorded in 2003 and kept for analysis. The background was estimated to 3112 (resp. 1994 and 1118) events according to the observed numbers of WS events.

5 K_{e4} kinematics

The decay $K^\pm \to \pi^+\pi^- e^\pm\nu$ is conveniently described using 3 different rest frames: the $K^\pm$ rest frame, the dipion rest frame and the dilepton rest frame. The kinematics is then fully described by the five Cabibbo–Maksymowicz variables [13, 14] as shown in the sketch of Fig. 1:

- $S_\pi = M^2_{\pi\pi}$, the invariant mass squared of the dipion
- $S_e = M^2_{e\nu}$, the invariant mass squared of the dilepton,
- θ_π, the angle of the $\pi^\pm$ in the dipion rest frame with respect to the flight direction of the dipion in the $K^\pm$ rest frame,
- θ_e, the angle of the $e^\pm$ in the dilepton rest frame with respect to the flight direction of the dilepton in the $K^\pm$ rest frame,
- ϕ, the angle between the dipion and dilepton rest frames.

The transition amplitude for K^+ can be written as:

$$\frac{G_w}{\sqrt{2}} V^*_{us} \langle \pi^+\pi^- | V^\lambda - A^\lambda | K^+ \rangle \bar{u}_\nu \gamma_\lambda (1-\gamma_5) v_e \,,$$

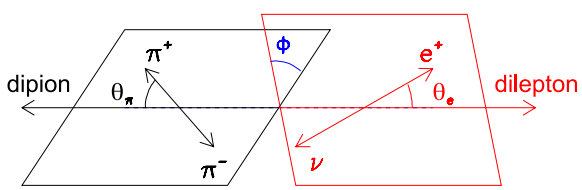

Fig. 1. Topology of the charged K_{e4} decay showing the angle definitions

where

$$\langle\pi^+\pi^-|A^\lambda|K^+\rangle = \frac{-\mathrm{i}}{m_K}\big(F(\mathbf{p}_{\pi^+}+\mathbf{p}_{\pi^-})^\lambda + G(\mathbf{p}_{\pi^+}-\mathbf{p}_{\pi^-})^\lambda + R(\mathbf{p}_e+\mathbf{p}_\nu)^\lambda\big) \quad \text{and}$$

$$\langle\pi^+\pi^-|V^\lambda|K^+\rangle = \frac{-H}{m_K^3}\epsilon^{\lambda\mu\rho\sigma}(\mathbf{p}_{\pi^+}+\mathbf{p}_{\pi^-}+\mathbf{p}_e+\mathbf{p}_\nu)_\mu \times(\mathbf{p}_{\pi^+}+\mathbf{p}_{\pi^-})_\rho(\mathbf{p}_{\pi^+}-\mathbf{p}_{\pi^-})_\sigma\,.$$

In the above expressions, $\mathbf{p}$ is the four-momentum of each particle and $\epsilon^{0123}=1$.

Three axial (F,G,R) and one vector (H) dimensionless complex form factors contribute to the transition amplitude and can be developed in partial wave expansion of s,p,d waves [15].

$$F = F_s\mathrm{e}^{\mathrm{i}\delta_s} + F_p\mathrm{e}^{\mathrm{i}\delta_p}\cos\theta_\pi + d\text{ wave}\ldots$$
$$G = G_p\mathrm{e}^{\mathrm{i}\delta_g} + d\text{ wave}\ldots$$
$$H = H_p\mathrm{e}^{\mathrm{i}\delta_h} + d\text{ wave}\ldots$$

The third axial form factor R is suppressed by a factor m_e^2/S_e. Consequently, there is no way to measure it in K_{e4} decays.

Neglecting d wave terms and assuming the same phase for F_p, G_p, H_p, only one phase and four real form factors are left ($\delta=\delta_s-\delta_p$, and F_s, F_p, G_p, H_p) which are expanded further [5] in powers of dimensionless invariants $q^2=\big(S_\pi/4m_\pi^2\big)-1$ and $S_e/4m_\pi^2$:

$$F_s = f_s + f_s'q^2 + f_s''q^4 + f_e'S_e/4m_\pi^2 + \ldots$$
$$F_p = f_p + f_p'q^2 + \ldots$$
$$G_p = g_p + g_p'q^2 + \ldots$$
$$H_p = h_p + h_p'q^2 + \ldots$$
$$\delta(q^2) = \delta_s - \delta_p\,.$$

As pointed out in [16], going from K^+ to K^- under CPT conservation, θ_e should be replaced by $\pi-\theta_e$, ϕ should be replaced by $\pi+\phi$ and H_p by $-H_p$. Under the assumption of CP conservation, this is equivalent to consider that the ϕ distribution of K^+ decays is opposite to the ϕ distribution of K^- decays with the same H_p value.

6 Monte Carlo simulation

Signal and background events were generated in the kaon rest frame according to a realistic decay matrix element and then boosted into the experimental reference frame. The incident kaon trajectory and momentum was generated according to the time variations of the beam geometry for each kaon charge and the decay vertex position according to the exponential decay law. As a precise knowledge of the acceptance and resolution in the five-dimensional space of the kinematic variables is necessary, a detailed GEANT3-based [17] Monte Carlo (MC) simulation was used, including full detector geometry and material description, DCH alignment and local inefficiencies. A large time-weighted MC production was achieved, providing a sample about 25 times larger than the data and reproducing the observed ratio $(K^+/K^-)=1.8$. The same reconstruction and selection codes as for data were used, except for the timing cuts. The effect of the LDA cut was applied to the simulated electron candidates as a momentum-dependent efficiency. This represents the optimal imple-

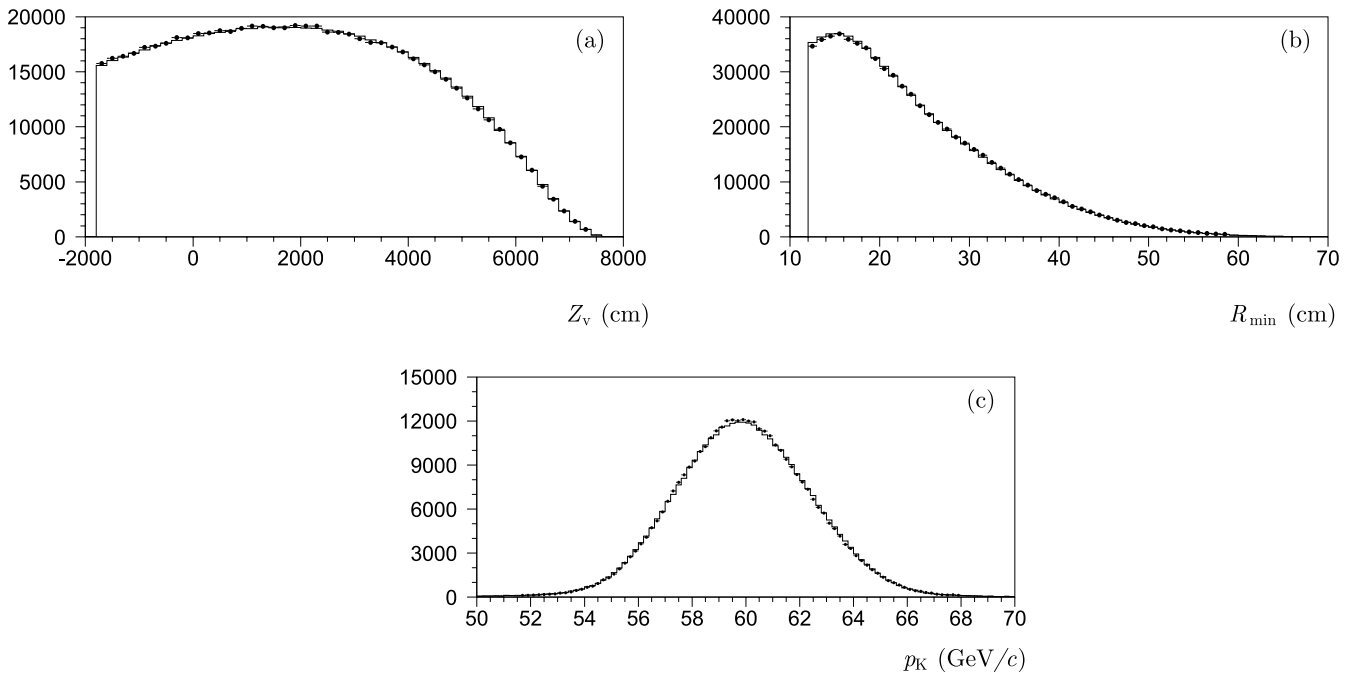

Fig. 2. Distribution of **a** the vertex longitudinal position, **b** the minimum track radius at DCH1, **c** the reconstructed kaon momentum. Data are shown as *points* with *error bars*, simulation as *histograms*

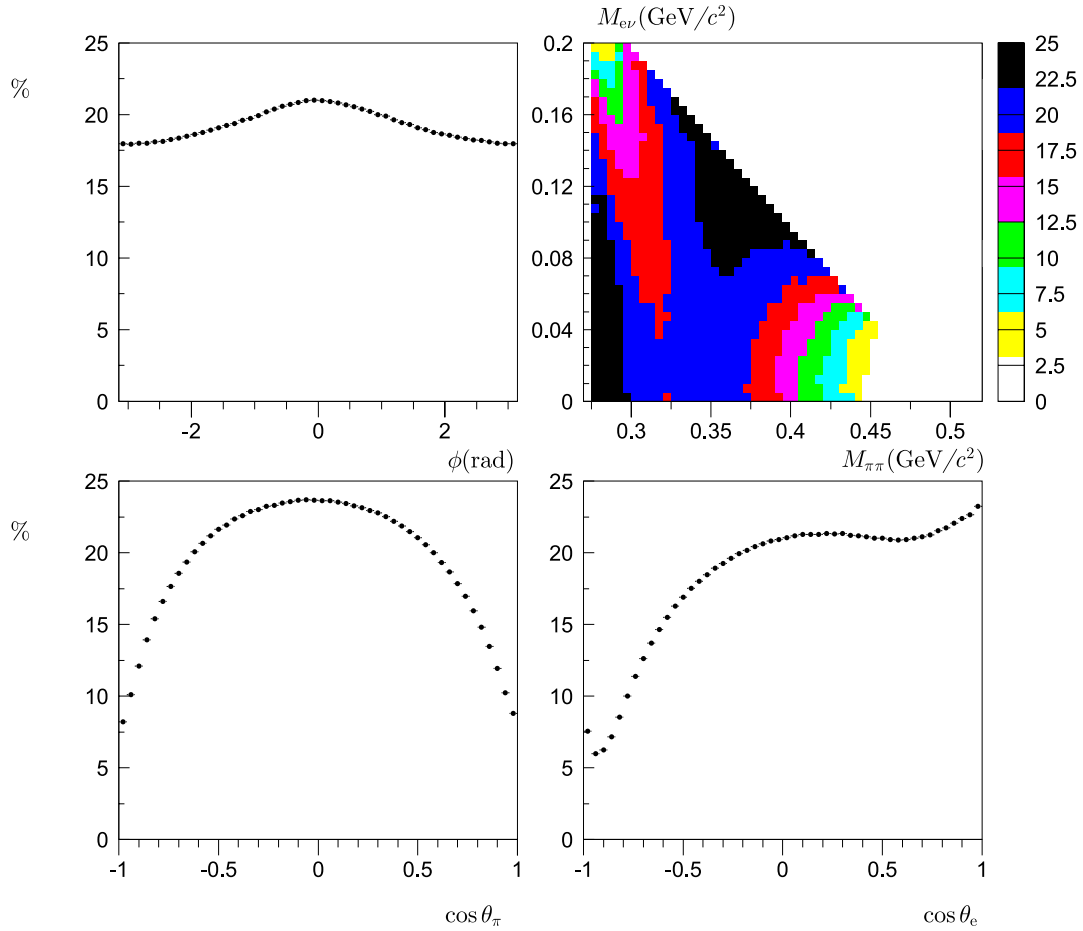

Fig. 3. Distribution of the acceptance (in %) as obtained from the simulation and projected in the $(M_{\pi\pi}, M_{e\nu})$ plane and along the 3 angular variables

mentation of the cut effect as it avoids to rely on the details of the shower developments, including fluctuations and limited statistics of the simulation. Two independent codes were used for the decay matrix element according to the Pais–Treiman formulation, one with a smooth phase shift variation [18] and constant form factors, the other with a phase shift variation following ChPT prediction [4] and form factors depending on invariant masses. They were used in independent analyses of the data.

The quality of the simulation can be seen from the plots of Fig. 2 where distributions of variables in the laboratory reference frame are shown for data and simulation. The experimental acceptances for the five Cabibbo–Maksymowicz variables are displayed in Fig. 3. The experimental resolutions are respectively:

$$\begin{aligned}
\sigma(M_{\pi\pi}) &= 0.0015\,\mathrm{GeV}/c^2\,, & \sigma(\cos\theta_\pi) &= 0.057\,,\\
\sigma(S_\pi) &= 0.000962\,(\mathrm{GeV}/c^2)^2\,, & \sigma(\theta_\pi) &= 71\,\mathrm{mrad}\,,\\
\sigma(M_{e\nu}) &= 0.0098\,\mathrm{GeV/c^2}\,, & \sigma(\cos\theta_e) &= 0.064\,,\\
\sigma(S_e) &= 0.001408\,(\mathrm{GeV}/c^2)^2\,, & \sigma(\theta_e) &= 80\,\mathrm{mrad}\,,\\
\sigma(\phi) &= 308\,\mathrm{mrad}\,.
\end{aligned}$$

Radiative corrections were implemented in the simulation in two successive steps:

– First the classical Coulomb attraction between the two opposite charge pions is applied by weighting the matrix element, according to the Gamow function:

$$C = \frac{\omega}{1-\mathrm{e}^{-\omega}}\,,$$

with $\omega = 2\pi\alpha/\beta$, where α is the fine structure constant and β the relative velocity expressed as $\beta = \frac{\sqrt{1-4v}}{1-2v}$ with $v = m_\pi^2/S_\pi$. The effect is mostly a distortion of the $M_{\pi\pi}$ spectrum near threshold.

– Second, real photons are generated by the program PHOTOS version 2.15 [19–21] interfaced to the simulation. Only 10% of the events have photons adding up to more than 1 GeV in the laboratory frame. The event selection furthermore reduces the acceptance for events with energetic photons. For these events, the resulting effect is a bias of the measured $M_{e\nu}$ and θ_e variables.

7 Analysis method

Following the Pais and Treiman formulation [15], one can write the decay probability as

$$d^5\Gamma = \frac{G_w^2 V_{us}^2}{(4\pi)^6 m_K^5}\rho(S_\pi, S_e) I(S_\pi, S_e, \cos\theta_\pi, \cos\theta_e, \phi) \times \mathrm{d}S_\pi\,\mathrm{d}S_e\,\mathrm{d}\cos\theta_\pi\,\mathrm{d}\cos\theta_e\,\mathrm{d}\phi\,,$$

where $\rho(S_\pi, S_e)$ is the phase space factor:

$$X\left(\frac{S_\pi - 4m_\pi^2}{S_\pi}\right)^{1/2}\left(1-\frac{m_e^2}{S_e}\right)^2,$$

with $X = \left(1/4\left(m_K^2 - S_\pi - S_e\right)^2 - S_\pi S_e\right)^{1/2}$. The function I can be expressed as the sum of 15 terms, each of them being the product of two terms, A_i which depends only on the form factor values and B_i which is only function of the kinematic variables:

$$I = \sum_{i=1}^{15} A_i(F_s, F_p, G_p, H_p, \delta) \times B_i(S_\pi, S_e, \cos\theta_\pi, \cos\theta_e, \phi)\,.$$

In K_{e4} decays, the electron mass is neglected and the term $\left(1-\frac{m_e^2}{S_e}\right)$ becomes unity.

One then defines a grid of equal population boxes in the five-variable space, adapted to the acceptance, resolution and dependence of the decay probability along each dimension. The chosen grid has ten bins in $M_{\pi\pi}$, five bins in $M_{e\nu}$, five bins in $\cos\theta_\pi$, five bins in $\cos\theta_e$ and twelve bins in ϕ, i.e. a total of 15 000 five-dimensional boxes. The number of data events per box is then 29 in the K^+ sample and 16 in the K^- sample which are analyzed separately as the simultaneous beam geometries are not identical. A dedicated estimator [6–8] is used in the fitting procedure to take into account Poisson fluctuations of the small number of events per box. This estimator reduces to the "classical" χ^2 definition for the already large number of events per box. In each of the boxes, the simulation allows to compute the average value of B_i, and the fitting procedure determines the best set of form factor values which minimizes the difference between the observed and expected number of events computed according to the current decay probability and summed over the 15 000 boxes.

In this analysis, the branching fraction is not measured, so only relative form factors are accessible: F_p/F_s, $G_p/F_s, H_p/F_s$ and the phase shift δ. Neglecting a possible $M_{e\nu}$ dependence and without prior assumption on the shape of their variation with $M_{\pi\pi}$, the form factors and phase shift are measured in independent $M_{\pi\pi}$ bins. As pointed out earlier [6], F_p/F_s and G_p/F_s are strongly correlated in the fitting procedure. To avoid undesirable large correlation effects, an intermediate quantity, $G'_p = G_p + \gamma/\alpha F_p$ is introduced and used in the fit, where

$$\alpha = \frac{1}{2m_K^2}\left(m_K^2 - S_\pi - S_e\right)\left(\frac{S_\pi - 4m_\pi^2}{S_\pi}\right)$$

and $\gamma = \frac{X}{m_K^2}$. All correlations are then within $\pm 20\%$ except the correlation between δ and G'_p/F_s which goes up to 40% at large $M_{\pi\pi}$. Fits are performed in the four-dimensional space, separately for the K^+ and K^- samples but using the same $M_{\pi\pi}$ bins definition. The results are checked for consistency and then combined in each bin according to their statistical weight. The relative normalizations ($N_{\rm Data}/N_{\rm MC}$) are proportional to F_s^2 and are rescaled to have a mean value equal to unity. Last, values of $F_p/F_s, G_p/F_s, H_p/F_s$ are deconvoluted of the observed F_s variation in each bin and plotted against $M_{\pi\pi}$ to investigate a possible further dependence.

In a second stage of the analysis, the observed variations of the form factors and phase shift with $M_{\pi\pi}$ are used to determine other parameter values through specific models.

8 Systematic uncertainties

Two independent analyses were performed on a large fraction of the 2003 data sample. They were based on different event selection and reconstruction, different detector corrections and different binning and fitting procedures. Consistent results were obtained, ensuring the robustness of the analysis.

Many items were investigated to assess possible biases in the results. For each of them, the analysis was repeated varying one condition at a time and a systematic uncertainty was quoted for each fitted parameter in each $M_{\pi\pi}$ bin. A particular attention was given to possible bin-to-bin correlations, observed for some effects. In most cases, the observed variation has a statistical origin and is conservatively quoted as a systematic uncertainty. When dealing with larger data statistics, these components decrease accordingly.

- Fitting procedure: The number of boxes used in the fitting procedure was varied within a factor 2, keeping the same definition for the 10 $M_{\pi\pi}$ bins. This last number was also extended to 12 and 15 bins. No visible bias was observed.
- Trigger efficiency: Two independent attempts to measure the high ($\sim 99.3\%$) trigger efficiency were made. The first one considers K_{e4} selected candidates satisfying the level 1 trigger condition (downscaled by 100 and thus suffering a lack of statistics) and measures the efficiency from events which satisfy the level 2 trigger. The second approach focuses on $K^\pm \to \pi^\pm\pi^0_D$ events satisfying the level 1 trigger condition, kinematic cuts and loose particle identification. Assigning a pion mass to both $\pi^\pm$ and opposite charge electron tracks allows to reach the full $M_{\pi\pi}$ range with sufficient statistics. Both methods have been used to apply the trigger efficiency in the five-dimensional space to the simulation. As the efficiency is almost uniform, the overall effect is marginal.
- Acceptance: The simulation is used to compute the acceptance in boxes of the five-dimensional space. It has been checked to be independent of the detailed physics assumptions provided that the whole phase space is covered. In addition, particular care was taken in controlling the geometrical acceptance and in following the time-dependence of the beam geometry. Many checks were performed to test the stability of the analysis, splitting the data in independent sub-samples according to the kaon charge, achromat polarity, dipole magnet polarity, decay vertex longitudinal position, spatial impact of the electron on the calorimeter front face and

Table 1. Contribution of the systematic errors (in 10^{-3} units) to each of the form factors. The background level and S_e dependence contributions are 100% bin-to-bin correlated

$\times 10^3$	fit method	trigger	acceptance	back. shape	e-ident.	rad. corr.	back. level	S_e dep.	total syst.
f'_s/f_s	0.4	2.5	1.2	2.5	1.8	1.1	3.1	2.6	±5.9
f''_s/f_s	0.2	2.3	1.2	2.2	1.5	1.4	2.4	5.2	±7.0
f'_e/f_s	1.6	0.1	1.0	2.7	0.2	2.7	6.8	4.1	±9.0
f_p/f_s	0.4	0.4	0.6	1.5	0.8	0.9	3.0	2.4	±4.3
g_p/f_s	1.3	0.9	2.0	5.5	2.8	3.5	8.5	4.4	±12.2
g'_p/f_s	1.7	1.3	2.6	6.8	3.4	6.9	9.3	4.5	±14.9
h_p/f_s	1.0	1.0	3.8	2.7	5.1	2.1	1.6	2.6	±8.0
a_0^0 (1p fit)	0.4	0.2	1.3	0.9	0.9	0.5	0.9	0.5	±2.2
a_0^0 (2p fit)	1.3	0.6	3.9	3.3	2.8	1.6	2.5	1.3	±6.9
a_0^2 (2p fit)	0.7	0.4	2.6	1.8	1.7	1.0	1.2	0.7	±4.1

data taking time. Results were compared in each bin and found to be consistent within the statistical errors.

– Background contamination: The analysis was repeated subtracting the "wrong sign" (WS) events according to their five-dimensional distributions, and scaled by a factor one, two or three. The dependence of each fitted parameter with the WS events scale factor was measured in each $M_{\pi\pi}$ bin. The scale factor for the background subtraction was cross-checked using a detailed simulation of contributing processes and found to be 2.0 ± 0.3. The effect of the 0.3 uncertainty is propagated to each point according to the measured slopes and quoted as systematic uncertainty (labeled background level in Table 1). The effect is bin-to-bin correlated, as expected.
The background in the five-dimensional space is not uniform but accumulates at low $M_{\pi\pi}$ values and around $M_{e\nu} = m_{\pi^+}$. Varying the semi-axes of the elliptic cut in the plane $(M_{3\pi}, p_t)$ accepts different fractions and shapes of the $K_{3\pi}$ background. Results were found to be stable with this cut without bin-to-bin correlation. Residual effects were quoted as systematic uncertainty (labeled background shape in Table 1).
– Electron identification: The final rejection against pions mis-identified as electrons ($E/p > 0.9$) is achieved by a cut on an LDA variable. In the simulation, the cut effect is applied as a momentum dependent efficiency. The cut value was varied from 0.85 to 0.90 (nominal cut) and 0.95. The analysis was repeated in the three conditions and the residual variation quoted as a systematic uncertainty.
– Radiative corrections: The effect of radiative corrections has been investigated on simulated data where the PHOTOS generation of photons was switched off. These events were subsequently processed in the same analysis chain as real data. The difference observed for each fitted parameter in each $M_{\pi\pi}$ bin between this simulation without PHOTOS and the same one using PHOTOS was thus evaluated and one tenth of the full effect was quoted as the theoretical uncertainty on the radiative corrections. This is based on detailed comparisons between PHOTOS and KLOR codes available in the $K_L \to \pi^\pm e^\mp \nu$ mode where a residual relative difference of 0.1% was observed [23], one tenth of the full PHOTOS effect.
– Dependence on S_e: As the dependence of the form factors with $M_{e\nu}$ was not considered in the first stage analysis, its potential effect was estimated by analyzing simulated events as real data, including a reweighting for $f'_e/f_s = 0.1$. The observed deviation, found bin-to-bin correlated, was quoted as a systematic uncertainty.

The impact of each considered item on the final set of parameters is shown in Table 1. The main sources of systematic uncertainties are the background contamination and electron identification for the form factors and the acceptance control for the phase measurements.

In addition, a different reconstruction of the Cabibbo–Maksymowicz variables, based on the information of the KABES detector to measure the kaon momentum and incident direction, lead to angular resolutions improved by $\sim 50\%$. However, as the information was only available for half of the event sample and subject to different systematic uncertainties (mis-tagging rate of few percent), this alternative analysis was used as a cross-check of the standard procedure and found in good agreement with statistical errors improved by 5 to 10%.

9 Results and interpretation

The detailed numerical results obtained in the ten independent bins of $M_{\pi\pi}$ are given in the Appendix (Tables 2–5). As explained in the previous section, the systematic uncertainties do have a bin-to-bin correlated component but much smaller than the uncorrelated one. In the tables, only the diagonal term of the matrix is quoted but the full error matrix for the ten values of δ is given in the Appendix (Table 6). The agreement between data and simulation after the fit can be seen in Fig. 4 which shows, for each kaon sign, the evolution of the individual ϕ distributions with the $M_{\pi\pi}$ bins. The overall agreement between data and simulated distributions is excellent for each of the five kinematic variables as can be seen from Fig. 5.

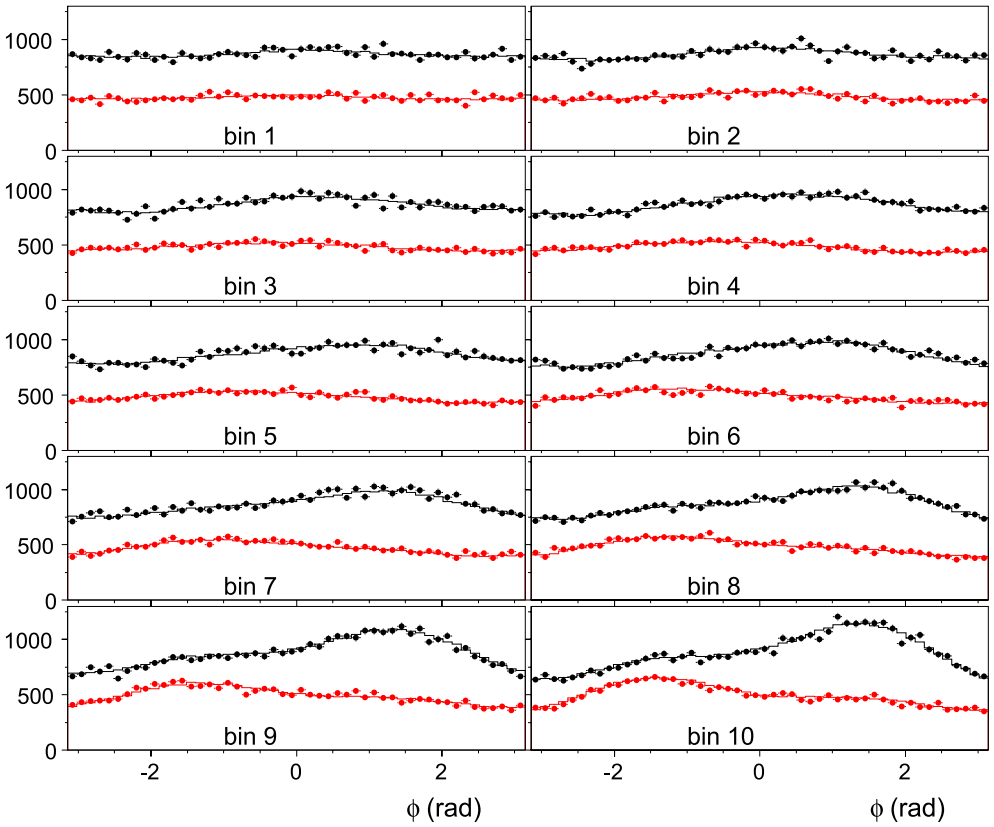

Fig. 4. Distribution of the ϕ angle for K^+ and K^- events in the ten $M_{\pi\pi}$ bins. In each plot, the *top (black) symbols* are the K^+ data, the *bottom (red) symbols* are the K^- data. The *histograms* are the simulation

The variation of the form factors is plotted against $M_{\pi\pi}$ in Fig. 6.

9.1 The F_s^2 form factor

A two-dimensional fit of the relative normalization data/MC $\left(\propto F_s^2\right)$ in the plane $(M_{\pi\pi}, M_{e\nu})$ is performed on a (10×10) grid using the polynomial form:

$$F_s = f_s\left(1 + f_s'/f_s q^2 + f_s''/f_s q^4 + f_e'/f_s S_e/4m_\pi^2\right) .$$

The correlations between the three slopes f_s'/f_s, f_s''/f_s and f_e'/f_s are given below:

	f_s'/f_s	f_s''/f_s	f_e'/f_s
f_s'/f_s	1.00	−0.96	0.08
f_s''/f_s		1.00	0.02
f_e'/f_s			1.00

The χ^2 of the fit is 102.3 for 79 degrees of freedom and blows up to 205.4 for 80 degrees of freedom if the S_e dependence is set to zero. The projections of the normalization on the $M_{\pi\pi}$ and $M_{e\nu}$ axis are shown in the top row of Fig. 6.

9.2 The F_p form factor

No evidence for a mass dependence is observed, thus a constant value is used. The χ^2 of the fit is 9.34 for 9 degrees of freedom. The small f_p/f_s measured value provides an a posteriori justification for neglecting the d wave terms.

9.3 The G_p form factor

A degree 1 polynomial in q^2 is used, neglecting a possible S_e dependence:

$$G_p/f_s = g_p/f_s + g_p'/f_s q^2 .$$

The correlation between g_p and g_p' is −0.91. The χ^2 of the fit is 8.23 for 8 degrees of freedom.

9.4 The H_p form factor

No evidence for a mass dependence is observed, thus a constant value is used. The χ^2 of the fit is 12.81 for 9 degrees of freedom.

9.5 Numerical results for the form factor measurements

The numerical results for all terms are given below:

$$\begin{aligned}
f_s'/f_s &= 0.172 \pm 0.009_{\rm stat} \pm 0.006_{\rm syst}\\
f_s''/f_s &= -0.090 \pm 0.009_{\rm stat} \pm 0.007_{\rm syst}\\
f_e'/f_s &= 0.081 \pm 0.008_{\rm stat} \pm 0.009_{\rm syst}\\
f_p/f_s &= -0.048 \pm 0.004_{\rm stat} \pm 0.004_{\rm syst}\\
g_p/f_s &= 0.873 \pm 0.013_{\rm stat} \pm 0.012_{\rm syst}\\
g_p'/f_s &= 0.081 \pm 0.022_{\rm stat} \pm 0.015_{\rm syst}\\
h_p/f_s &= -0.411 \pm 0.019_{\rm stat} \pm 0.008_{\rm syst} .
\end{aligned}$$

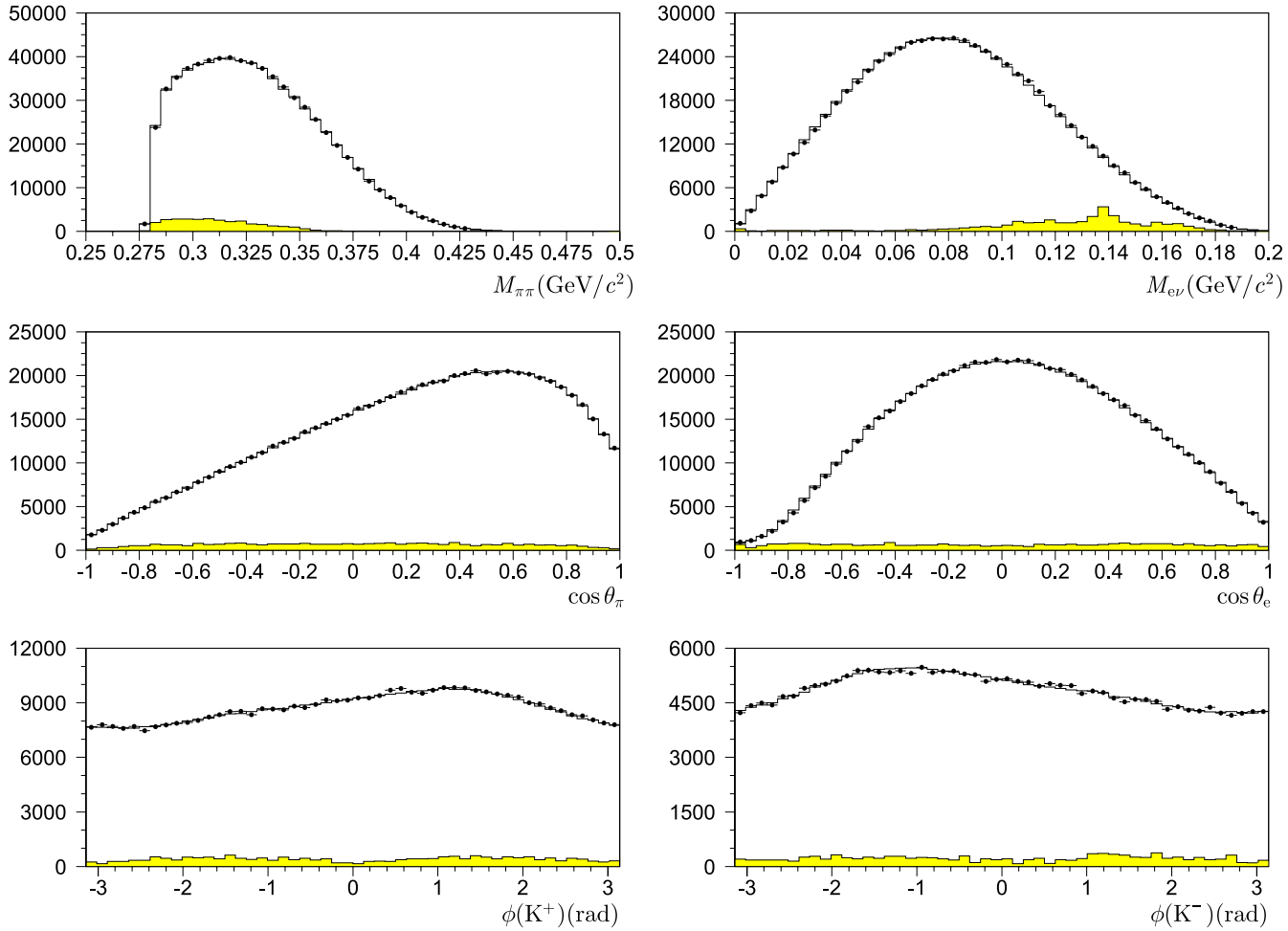

Fig. 5. Distribution of the five Cabibbo–Maksymowicz variables as observed in the detector. The ϕ distributions are shown separately for K^+ and K^- to emphasize their opposite behavior. Data (after background subtraction) are shown as *symbols with error bars*, simulation using the fitted form factor values as *histograms*. The background contribution (WS events) is superimposed in the *shaded area*, increased by a factor of 10 to be visible on the linear scale

9.6 The δ phase shift

The phase shift measurements are shown in Fig. 7 together with results from previous experiments [6–8]. All data are in agreement (except maybe the highest data point from E865). At this stage of the analysis, the phase shift measurements do not rely on the $\pi\pi$ scattering amplitude through a specific model and can be compared to theoretical predictions already available or still under development.

Under isospin symmetry assumption, the phase shift measurements can be related to the $\pi\pi$ scattering lengths using the analytical properties of the $\pi\pi$ scattering amplitudes and crossing symmetry relating amplitudes with different isospin (Roy equations). Several approaches [2, 3, 22] have been developed to extract numerical values for a_0^0 (and a_0^2) from phase measurements using K_{e4} data alone or combined with other $\pi\pi$ scattering experimental data. In this paper, we use conservatively (but arbitrarily) the Universal Band (UB) approach [2] and NA48/2 K_{e4} data alone, extracting first the single variable a_0^0 (expressed in units of m_{π^+}). Figure 8 shows the UB boundaries in the plane (a_0^2, a_0^0), the width of the band reflecting the uncertainty on the external input data at $M_{\pi\pi} > 0.8\,\mathrm{GeV}/c^2$ used in the predictions. Scanning through the band, the preferred values (a_0^0, a_0^2) are found and the fit χ^2 favors the region of low scattering lengths values as it decreases from 14.9 to 9.2 for nine degrees of freedom from top to bottom boundary. At the center line of the Universal Band (1-parameter fit), NA48/2 phase measurements translate as:

$$a_0^0 = 0.256 \pm 0.006_{\mathrm{stat}} \pm 0.002_{\mathrm{syst}}{}^{+0.018}_{-0.017_{\mathrm{ext}}}\,,$$

which implies

$$a_0^2 = -0.0312 \pm 0.0011_{\mathrm{stat}} \pm 0.0004_{\mathrm{syst}}{}^{+0.0129}_{-0.0122_{\mathrm{ext}}}\,.$$

The external uncertainties correspond to the change in a_0^0 and a_0^2 when moving from the center line to the top (resp. bottom) boundary of the band. Figure 8 shows the

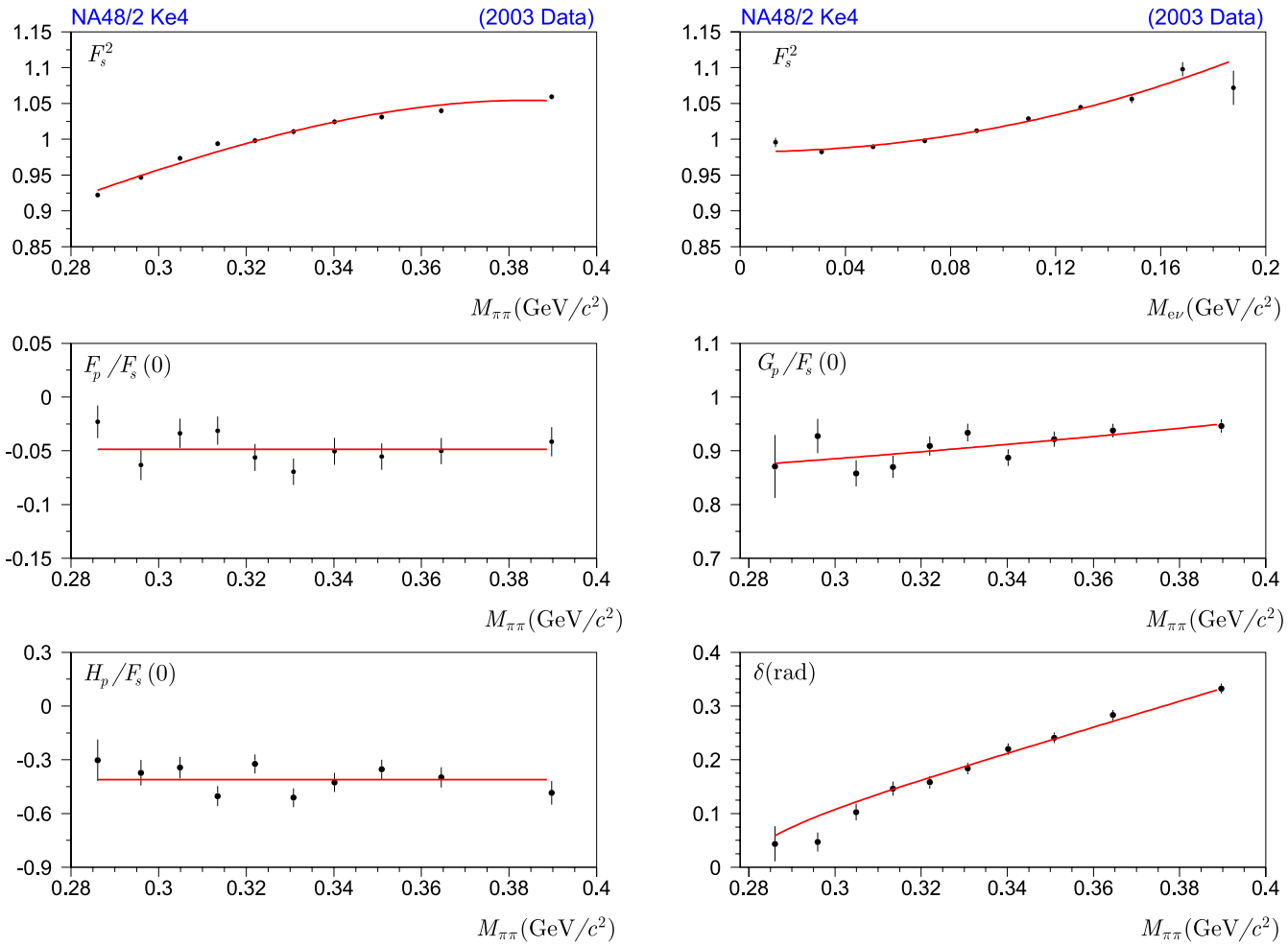

Fig. 6. Variation of the fitted form factors and phase shift with $M_{\pi\pi}$. *Top row*: F_s^2 projected on the $M_{\pi\pi}$-axis assuming no S_e dependence and residual dependence when projected on the $M_{e\nu}$-axis. *Mid row*: $F_p/F_s(0)$ and $G_p/F_s(0)$. *Bottom row*: $H_p/F_s(0)$ and phase shift δ. In the last plot, the *line* corresponds to a 1-parameter fit using the universal band *center line* constraint

results together with a two-parameter fit where both a_0^0 and a_0^2 are free parameters:

$$a_0^0 = 0.233 \pm 0.016_{\mathrm{stat}} \pm 0.007_{\mathrm{syst}}\,,$$
$$a_0^2 = -0.0471 \pm 0.011_{\mathrm{stat}} \pm 0.004_{\mathrm{syst}}\,.$$

The quoted errors correspond to the diagonal terms of the 1-σ error matrix which exhibits a large 96.7% correlation in the non-diagonal term. The universal band interpretation of the K_{e4} phase measurements favors a much higher value than the quite precise ChPT prediction of [4] ($a_0^0 = 0.220 \pm 0.005, a_0^2 = -0.0444 \pm 0.0010$).

However, recent work ([24, 25] and references therein) suggests that additional isospin symmetry breaking effects, generated by the pion and quark mass differences and neglected so far in the K_{e4} phase shift evaluation, are of the order of 10 to 15 mrad over the full accessible range and would thus lead, when taken into account, to substantially smaller a_0^0 and a_0^2 extracted values, as shown in Fig. 8. The isospin corrected values would be decreased from 0.256 to 0.238 (resp. -0.0312 to -0.0347) for a_0^0 (resp. a_0^2) at the center line of the universal band. Similar shifts would be

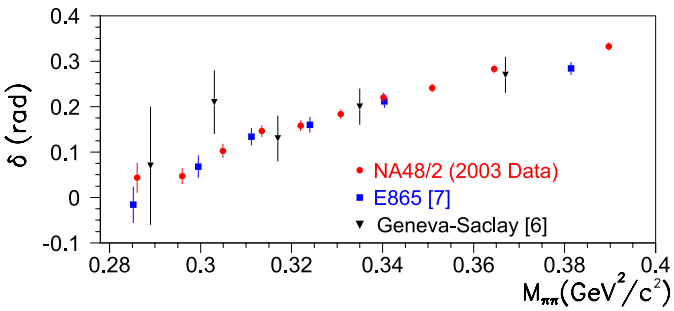

Fig. 7. Phase shift (δ) measurements from the three K_{e4} experiments against $M_{\pi\pi}$

observed if other constraints were used. The experimental statistical and systematic uncertainties are unaffected while the additional uncertainty from isospin corrections is expected to be smaller. Such corrections were not applied in the data analysis of previous K_{e4} experiments. However, as both experiments published their results in the independent-bin analysis, these isospin breaking cor-

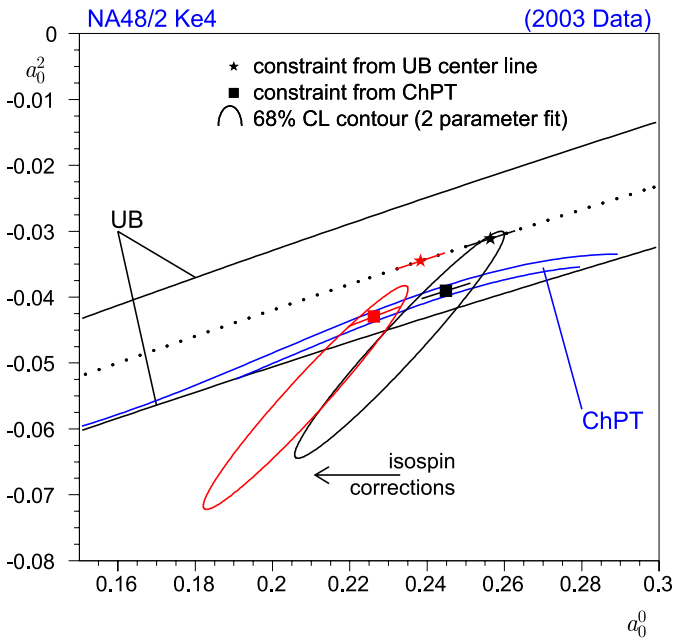

Fig. 8. Results for the $\pi\pi$ scattering lengths a_0^0 and a_0^2 (in m_{π^+} unit) from fits to the NA48/2 K_{e4} data using different theoretical assumptions. The *black solid curves* are the universal band boundaries (Roy equations), the narrow blue band is the restricted area using the ChPT constraint. The *symbols* correspond to the results of 1-parameter fits to the data: the *star* is the value obtained at the center line of the universal band (*dotted line*), the *square* using the ChPT constraint. The error bars are 1-σ errors. The contour corresponds to 68% CL in a two-parameter fit. The whole picture is translated towards lower values of the scattering lengths when (preliminary) isospin symmetry breaking corrections [24, 25] are considered

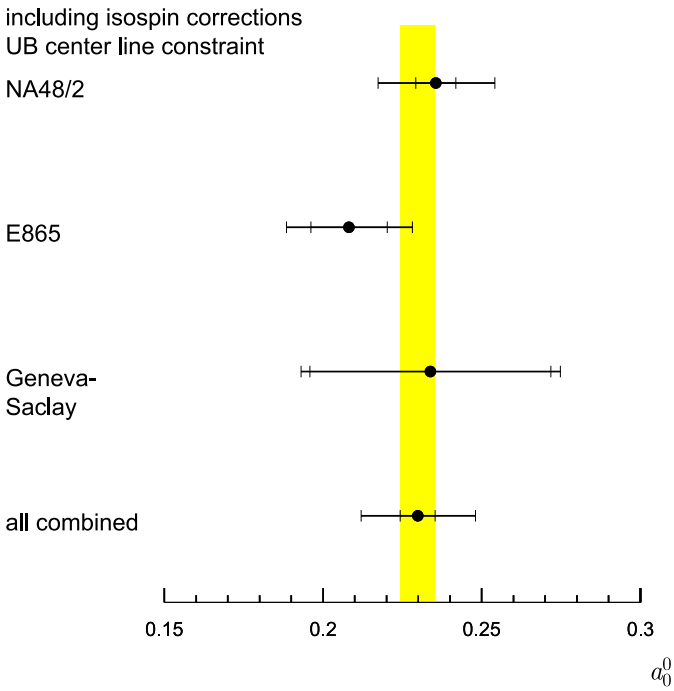

Fig. 9. Results of the a_0^0 scattering length measurement using the constraint from Universal Band center line after isospin corrections [24, 25] have been applied. The error bars correspond to the experimental (first tick mark) and total (second tick mark) errors (obtained by adding in quadrature the experimental and theoretical uncertainties). In the combined result, the experimental errors are uncorrelated between experiments while the theoretical errors are fully correlated

rections can be applied a posteriori to all experiments as shown in Fig. 9. The NA48/2 K_{e4} value is then consistent with values of $(a_0^0 - a_0^2)$ and a_0^2 obtained from the study of a cusp-like structure in the $K^\pm \to \pi^0\pi^0\pi^\pm$ decays [26, 27] and precise predictions from ChPT. Any attempt to combine measurements from the three K_{e4} experiments will be dominated by the NA48/2 improved accuracy and larger sensitivity due to the higher accessible $M_{\pi\pi}$ range.

10 Summary

The axial and vector form factors of the K_{e4} decays have been measured with an unprecedented relative precision of few percent. The s wave contribution to the F form factor has been measured to be mostly linear with S_π with additional slopes with S_e and S_π^2. A negative $\sim 5\%$ p wave contribution to F has been established while a linear (resp. constant) behavior with S_π for the G (resp. H) form fac-

Table 2. Definition of the ten bins in $M_{\pi\pi}$: bin range, event numbers $(K^+ + K^-)$, barycenter and χ^2 of the fits for (2×1496) degrees of freedom

bin number	$M_{\pi\pi}$ range (MeV/c^2)	Number of events $(K^+ + K^-)$	$\langle M_{\pi\pi} \rangle$ (MeV/c^2)	χ^2
1	279.00 – 291.29	43 359 + 23 753	286.07	3146.42
2	291.29 – 300.50	43 304 + 24 022	295.97	3109.80
3	300.50 – 309.22	43 288 + 24 071	304.89	3037.69
4	309.22 – 317.73	43 370 + 24 185	313.47	3172.82
5	317.73 – 326.35	43 500 + 24 069	322.02	3006.71
6	326.35 – 335.33	43 564 + 24 272	330.78	2881.01
7	335.33 – 345.25	43 667 + 23 845	340.17	3015.82
8	345.25 – 357.03	43 769 + 24 331	350.92	2982.36
9	357.03 – 373.27	43 887 + 24 712	364.52	2914.61
10	> 373.27	43 946 + 24 596	389.71	3019.57

Table 3. Result of the fits for $F_s^2/F_s^2(0)$ (neglecting a possible $M_{e\nu}$ dependence) and $F_p/F_s(0)$. The quoted systematic errors correspond to the bin-to-bin uncorrelated part only

bin	$F_s^2/F_s^2(0)$ value	statistical error	systematic error	$F_p/F_s(0)$ value	statistical error	systematic error
1	0.9221	0.0036	0.0026	−0.0229	0.0151	0.0022
2	0.9467	0.0037	0.0016	−0.0633	0.0140	0.0072
3	0.9737	0.0038	0.0020	−0.0337	0.0135	0.0092
4	0.9938	0.0039	0.0018	−0.0312	0.0132	0.0078
5	0.9982	0.0039	0.0012	−0.0561	0.0125	0.0068
6	1.0106	0.0040	0.0016	−0.0696	0.0123	0.0085
7	1.0241	0.0040	0.0010	−0.0504	0.0125	0.0093
8	1.0312	0.0040	0.0015	−0.0554	0.0122	0.0028
9	1.0397	0.0041	0.0018	−0.0502	0.0122	0.0038
10	1.0593	0.0041	0.0053	−0.0415	0.0135	0.0051

Table 4. Result of the fits for $G_p/F_s(0)$ and $H_p/F_s(0)$. The quoted systematic errors correspond to the bin-to-bin uncorrelated part only

bin	$G_p/F_s(0)$ value	statistical error	systematic error	$H_p/F_s(0)$ value	statistical error	systematic error
1	0.8708	0.0584	0.0091	−0.3026	0.1164	0.0381
2	0.9274	0.0319	0.0176	−0.3726	0.0718	0.0276
3	0.8580	0.0243	0.0180	−0.3431	0.0601	0.0205
4	0.8700	0.0207	0.0102	−0.5027	0.0558	0.0142
5	0.9089	0.0180	0.0113	−0.3226	0.0534	0.0118
6	0.9338	0.0164	0.0117	−0.5117	0.0530	0.0154
7	0.8874	0.0155	0.0122	−0.4262	0.0533	0.0150
8	0.9218	0.0141	0.0040	−0.3532	0.0541	0.0213
9	0.9376	0.0129	0.0044	−0.3981	0.0569	0.0462
10	0.9462	0.0124	0.0051	−0.4846	0.0653	0.0300

tor has been observed, in good agreement with predictions from ChPT [5].

The phase shift δ has been determined in an independent-bin analysis which allows comparison and combination with earlier measurements. The relation between δ values and the $\pi\pi$ scattering lengths a_0^0 and a_0^2 is subjected to theoretical external inputs whose uncertainties are now larger than the improved NA48/2 experimental accuracy. In particular, isospin symmetry was assumed in the relation to scattering lengths. This opens the way to new interesting developments, competitive with the achieved accuracy of the experimental measurement: $a_0^0 = 0.256 \pm 0.006_{\rm stat} \pm 0.002_{\rm syst}{}^{+0.018}_{-0.017{\rm ext}}$, which implies $a_0^2 = -0.0312 \pm 0.0011_{\rm stat} \pm 0.0004_{\rm syst}{}^{+0.013}_{-0.012{\rm ext}}$ if the constraint between a_0^0 and a_0^2 at the center line of the Universal Band is used; and $a_0^0 = 0.233 \pm 0.016_{\rm stat} \pm 0.007_{\rm syst}$, $a_0^2 = -0.0471 \pm 0.011_{\rm stat} \pm 0.004_{\rm syst}$ and a 96.7% correlation if both scattering lengths are taken as independent parameters. Promising theoretical work to include isospin symmetry breaking effects suggests that those values could then be decreased by ~ 0.02 for a_0^0 and by ~ 0.004 for a_0^2, bringing the measurement in agreement with other measurements from NA48/2 and with predictions from ChPT.

Appendix: Fit results for independent $M_{\pi\pi}$ bins

The following tables give the definition of the $M_{\pi\pi}$ bins (Table 2) and the fit results for the four form factors (Tables 3 and 4) and δ phase shift (Table 5).

Table 5. Result of the fits for the phase shift δ (mrad). The quoted systematic errors correspond to the bin-to-bin uncorrelated part only

bin	δ value (mrad)	statistical error (mrad)	systematic error (mrad)
1	43.430	32.706	12.328
2	46.931	17.769	4.769
3	102.715	15.212	5.382
4	146.341	13.278	4.303
5	158.153	11.653	5.978
6	183.840	10.801	5.355
7	219.941	10.789	3.761
8	241.119	9.975	3.065
9	283.125	9.566	1.057
10	332.535	9.155	3.050

Table 6. Full error matrix between δ values (in $(\text{mrad})^2$), including all statistical and systematic errors. The bin-to-bin correlated errors appear in the non-diagonal terms

bin	1	2	3	4	5	6	7	8	9	10
1	1221.62	0.50	0.60	1.68	1.60	1.34	2.49	1.53	0.19	0.16
2	0.50	338.46	0.43	0.54	0.64	0.43	0.62	0.41	0.14	0.08
3	0.60	0.43	260.38	0.62	0.71	0.49	0.73	0.48	0.15	0.09
4	1.68	0.54	0.62	194.83	1.40	1.12	1.99	1.23	0.20	0.15
5	1.60	0.64	0.71	1.40	171.53	1.13	1.92	1.20	0.23	0.16
6	1.34	0.43	0.49	1.12	1.13	145.34	1.60	0.99	0.16	0.12
7	2.49	0.62	0.73	1.99	1.92	1.60	130.54	1.80	0.23	0.20
8	1.53	0.41	0.48	1.23	1.20	0.99	1.80	108.89	0.15	0.13
9	0.19	0.14	0.15	0.20	0.23	0.16	0.23	0.15	92.63	0.03
10	0.16	0.08	0.09	0.15	0.16	0.12	0.20	0.13	0.03	93.12

To take into account correctly the bin-to-bin correlations of some of the systematic uncertainties, a complete treatment using a covariance matrix has been implemented. The statistical errors and the bin-to-bin uncorrelated systematic errors are added in quadrature in the diagonal terms σ_{ii}^2 of a (10×10) error matrix. The non-diagonal terms σ_{ij}^2 are filled with $\rho\,\sigma_i\sigma_j$, ρ being the correlation coefficient, here taken equal to unity. The error matrix (Table 6) is to be inverted to get the covariance matrix (V) and used in the χ^2 calculation when extracting values of a set of parameters (a) using a dedicated function $y(a)$:

$$\chi^2 = \sum_{i,j} (x_i - y_i(a))^{\mathrm{T}} V_{ij} (x_j - y_j(a)) \,,$$

where x is the vector of measured values, $y(a)$ is the vector of fitted values for parameter(s) a and V the covariance matrix of the measurements.

Acknowledgements. We gratefully acknowledge the CERN SPS accelerator and beam-line staff for the excellent performance of the beam and the technical staff of the participating laboratories and universities for their effort in the maintenance and operation of the detectors. We would like also to thank the theory groups from Bern, Orsay, Marseille and Madrid for fruitful discussions and in particular J. Gasser and J. Stern for their interest in the progresses of the analysis and their time investment in further developments.

References

1. S. Roy, Phys. Lett. B **36**, 353 (1971)
2. B. Ananthanarayan, G. Colangelo, J. Gasser, H. Leutwyler, Phys. Rep. **353**, 207 (2001)
3. S. Descotes, N. Fuchs, L. Girlanda, J. Stern, Eur. Phys. J. C **24**, 469 (2002)
4. G. Colangelo, J. Gasser, H. Leutwyler, Nucl. Phys. B **603**, 125 (2001)
5. G. Amoros, J. Bijnens, J. Phys. G **25**, 1607 (1999)
6. L. Rosselet et al., Phys. Rev. D **15**, 574 (1977)
7. S. Pislak et al., Phys. Rev. Lett. **87**, 221 801 (2001)
8. S. Pislak et al., Phys. Rev. D **67**, 072 004 (2003)
9. J. Batley et al., Phys. Lett. B **634**, 474 (2006)
10. J. Batley et al., Phys. Lett. B **638**, 22 (2006)
11. V. Fanti et al., Nucl. Instrum. Methods A **574**, 433 (2007)
12. B. Peyaud, Nucl. Instrum. Methods A **535**, 247 (2004)
13. N. Cabibbo, A. Maksymowicz, Phys. Rev. **137**, B438 (1965)
14. N. Cabibbo, A. Maksymowicz, Phys. Rev. **168**, 1926 (1968)
15. A. Pais, S. Treiman, Phys. Rev. **168**, 1858 (1968)
16. T.D. Lee, C.S. Wu, Ann. Rev. Nucl. Sci. **16**, 471 (1966)
17. GEANT Description and Simulation Tool, CERN Program Library Long Writeup W 5013, 1994
18. J.L. Basdevant, C.D. Froggatt, J.L. Petersen, Nucl. Phys. B **72**, 413 (1974)
19. E. Barberio, Z. Was, PHOTOS, Comput. Phys. Commun. **79**, 291 (1994)
20. G. Nanava, Z. Was, Eur. Phys. J. C **51**, 569 (2007)
21. P. Golonka, Z. Was, Eur. Phys. J. C **45**, 97 (2006)
22. J.R. Pelaez, F.J. Yndurain, Phys. Rev. D **71**, 074 016 (2005)
23. A. Lai et al., Phys. Lett. B **645**, 26 (2007)
24. J. Gasser, talk and contribution to the proceedings of KAON'07 conference, Frascati, May 2007 (arXiv:hep-ph/0710.3048)
25. J. Gasser, talk given at MENU 2007 conference, Jülich, September 2007, contribution to appear in the proceedings
26. J. Batley et al., Phys. Lett. B **633**, 173 (2006)
27. E. Goudzovski, talk and contribution to the proceedings of KAON'07 conference, Frascati, May 2007 [arXiv:hep-ex/0706.4059v3]